Title
Collective electric and magnetic plasmonic resonances in spherical nanoclusters

Journal
Optics Express, 19(3)

ISSN
1094-4087

Authors
Vallecchi, Andrea
Albani, Matteo
Capolino, Filippo

Publication Date
2011-01-28

DOI
10.1364/OE.19.002754

Collective electric and magnetic plasmonic resonances in spherical nanoclusters

Andrea Vallecchi,[1,*] Matteo Albani,[1] and Filippo Capolino[2]

[1]*Department of Information Engineering, University of Siena, Via Roma 56, 53100 Siena, Italy*

[2]*Department of Electrical Engineering and Computer Science, University of California-Irvine, Irvine, California 29697, USA*

**andrea.vallecchi@unisi.it*

Abstract: We report an investigation on the optical properties of three-dimensional nanoclusters (NCs) made by spherical constellations of metallic nanospheres arranged around a central dielectric sphere, which can be realized and assembled by current state-of-the-art nanochemistry techniques. This type of NCs supports collective plasmon modes among which the most relevant are those associated with the induced electric and magnetic resonances. Combining a single dipole approximation for each nanoparticle and the multipole spherical-wave expansion of the scattered field, we achieve an effective characterization of the optical response of individual NCs in terms of their scattering, absorption, and extinction efficiencies. By this approximate model we analyze a few sample NCs identifying the electric and magnetic resonance frequencies and their dependence on the size and number of the constituent nanoparticles. Furthermore, we discuss the effective electric and magnetic polarizabilities of the NCs, and their isotropic properties. A homogenization method based on an extension of the Maxwell Garnett model to account for interaction effects due to higher order multipoles in dense packed arrays is applied to a distribution of NCs showing the possibility of obtaining metamaterials with very large, small, and negative values of permittivity and permeability, and even negative index.

OCIS codes: (160.1245) Materials: Artificially engineered materials; (160.3918) Materials: Metamaterials; (240.6680) Optics at surfaces: Surface plasmons; (260.2065) Physical optics: Effective medium theory; (350.3618) Other areas of optics: Left-handed materials.

References and links

1. V. Ponsinet, A. Aradian, P. Barois, and S. Ravaine, "Self-assembly and nanochemistry techniques towards the fabrication of metamaterials," in Applications of Metamaterials, Ed. F. Capolino, CRC Press, Boca Raton, FL, 2009, Chap. 32.
2. J. B. Pendry, "Negative refraction makes a perfect lens," Phys. Rev. Lett. **85**(18), 3966–3969 (2000).
3. N. Fang, H. Lee, C. Sun, and X. Zhang, "Sub-diffraction-limited optical imaging with a silver superlens," Science **308**(5721), 534–537 (2005).
4. D. Schurig, J. J. Mock, B. J. Justice, S. A. Cummer, J. B. Pendry, A. F. Starr, and D. R. Smith, "Metamaterial electromagnetic cloak at microwave frequencies," Science **314**(5801), 977–980 (2006).
5. Q. Xu, R. M. Rioux, M. D. Dickey, and G. M. Whitesides, "Nanoskiving: a new method to produce arrays of nanostructures," Acc. Chem. Res. **41**(12), 1566–1577 (2008).
6. H. O. Moser, B. D. F. Casse, O. Wilhelmi, and B. T. Saw, "Terahertz response of a microfabricated rod-split-ring-resonator electromagnetic metamaterial," Phys. Rev. Lett. **94**(6), 063901 (2005).
7. N. Liu, H. Guo, L. Fu, S. Kaiser, H. Schweizer, and H. Giessen, "Three-dimensional photonic metamaterials at optical frequencies," Nat. Mater. **7**(1), 31–37 (2008).
8. V. M. Shalaev, W. Cai, U. K. Chettiar, H. K. Yuan, A. K. Sarychev, V. P. Drachev, and A. V. Kildishev, "Negative index of refraction in optical metamaterials," Opt. Lett. **30**(24), 3356–3358 (2005).
9. G. Dolling, M. Wegener, C. M. Soukoulis, and S. Linden, "Negative-index metamaterial at 780 nm wavelength," Opt. Lett. **32**(1), 53–55 (2007).
10. A. Alù, A. Salandrino, and N. Engheta, "Negative effective permeability and left-handed materials at optical frequencies," Opt. Express **14**(4), 1557–1567 (2006).

#137799 - $15.00 USD Received 8 Nov 2010; revised 18 Jan 2011; accepted 18 Jan 2011; published 28 Jan 2011

11. Y. A. Urzhumov, G. Shvets, J. A. Fan, F. Capasso, D. Brandl, and P. Nordlander, "Plasmonic nanoclusters: a path towards negative-index metafluids," Opt. Express **15**(21), 14129–14145 (2007).
12. C. R. Simovski, and S. A. Tretyakov, "Model of isotropic resonant magnetism in the visible range based on core-shell clusters," Phys. Rev. B **79**(4), 045111 (2009).
13. A. Alù, and N. Engheta, "The quest for magnetic plasmons at optical frequencies," Opt. Express **17**(7), 5723–5730 (2009).
14. J. A. Fan, C. Wu, K. Bao, J. Bao, R. Bardhan, N. J. Halas, V. N. Manoharan, P. Nordlander, G. Shvets, and F. Capasso, "Self-assembled plasmonic nanoparticle clusters," Science **328**(5982), 1135–1138 (2010).
15. C. F. Bohren, and D. R. Huffman, *Absorption and scattering of light by small particles* (Wiley, New York, 1983).
16. S. Steshenko, and F. Capolino, "Single dipole approximation for modeling collections of nanoscatterers" in *Theory and Phenomena of Metamaterials*, Ed. F. Capolino, (CRC Press, Boca Raton, FL, 2009), Chap. 8.
17. J. E. Hansen, *Spherical Near-Field Antenna Measurements* (Peter Peregrinus Ltd, London, 1988).
18. J. C. Love, L. A. Estroff, J. K. Kriebel, R. G. Nuzzo, and G. M. Whitesides, "Self-assembled monolayers of thiolates on metals as a form of nanotechnology," Chem. Rev. **105**(4), 1103–1169 (2005).
19. J. Israelachvili, *Intermolecular and surface forces*, Academic Press (2007).
20. S. Reculusa, C. Poncet-Legrand, S. Ravaine, C. Mingotaud, E. Duguet, and E. Bourgeat-Lami, "Synthesis of raspberry-like silica/polystyrene materials," Chem. Mater. **14**(5), 2354–2359 (2002).
21. J.-C. Taveau, D. Nguyen, A. Perro, S. Ravaine, E. Duguet, A. Brisson, and O. Lambert, "New insights into the nucleation and growth of PS nodules on silica nanoparticles by 3D cryo-electron tomography," Soft Matter **4**(2), 311–315 (2008).
22. B. W. Clare, and D. L. Kepert, "The closest packing of equal circles on a sphere," Proc. R. Soc. Lond. A Math. Phys. Sci. **405**(1829), 329–344 (1986).
23. J. R. Edmundson, "The distribution of point charges on the surface of a sphere," Acta Crystallogr. A **48**(1), 60–69 (1992).
24. D. A. Kottwitz, "The densest packing of equal circles on a sphere," Acta Crystallogr. A **47**(3), 158–165 (1991).
25. A. Ishimaru, S. W. Lee, Y. Kuga, and V. Jandhyala, "Generalized constitutive relations for metamaterials based on the quasi-static Lorentz theory," IEEE Trans. Antenn. Propag. **51**(10), 2550–2557 (2003).
26. M. Wheeler, J. Aitchison, and M. Mojahedi, "Coupled magnetic dipole resonances in sub-wavelength dielectric particle clusters," J. Opt. Soc. Am. B **27**(5), 1083–1091 (2010).
27. D. Mackowski, "Calculation of total cross sections of multiple-sphere clusters," J. Opt. Soc. Am. A **11**(11), 2851–2861 (1994).
28. I. Romero, J. Aizpurua, G. W. Bryant, and F. J. García De Abajo, "Plasmons in nearly touching metallic nanoparticles: singular response in the limit of touching dimers," Opt. Express **14**(21), 9988–9999 (2006).
29. K. Aydin, I. Bulu, K. Guven, M. Kafesaki, C. M. Soukoulis, and E. Ozbay, "Investigation of magnetic resonances for different split-ring resonator parameters and designs," N. J. Phys. **7**, 168 (2005).
30. O. N. Singh, and A. Lakhtakia, eds., *Electromagnetic Waves in Unconventional Materials and Structures* (John Wiley, New York, 2000).
31. P. C. Waterman, and N. E. Pedersen, "Electromagnetic scattering by periodic arrays of particles," J. Appl. Phys. **59**(8), 2609 (1986).
32. A. Moroz, and C. Sommers, "Photonic band gaps of three-dimensional face-centred cubic lattices," J. Phys. Condens. Matter **11**(4), 997–1008 (1999).
33. A. Moroz, "Metallo-dielectric diamond and zinc-blende photonic crystals," Phys. Rev. B **66**(11), 115109 (2002).
34. V. Yannopapas, and A. Moroz, "Negative refractive index metamaterials from inherently non-magnetic materials for deep infrared to terahertz frequencies," J. Phys. Condens. Matter **17**(25), 3717–3734 (2005).
35. S. Tretyakov, *Analytical Modeling in Applied Electromagnetics* (Artech House, 2003).

1. Introduction

Modern nanochemistry has developed efficient techniques to manipulate nanoscale objects with a highly advanced degree of control. Chemically-engineered nanoparticles can be synthesized with a large choice of sizes, shapes, constituent materials and surface coatings, and further assembled spatially into self-assembled structures, either spontaneously or in a directed manner [1]. Advances in particle self-assembly and the nearly unlimited range of nanostructures with controlled architectures and functions available suggest that such assemblies may also provide a simple route to metamaterials at infrared and visible length scales. Indeed, nanochemistry and self-assembly strategies are able to inexpensively produce fully three-dimensional (3D) metamaterials whose inner structure is natively in the right range of sizes for optical and infrared applications. The ability of bottom-up techniques to fabricate photonic metamaterials paves the way for turning into practice some of the exciting applications envisioned for metamaterials operating at visible wavelengths, such as the perfect lens and the invisibility cloak [2–4], to mention a few.

As a matter of fact, top-down methods such as electron beam lithography, direct laser writing, and nanoskiving [5] are suitable for fabricating plasmonic nanostructures on planar

#137799 - $15.00 USD Received 8 Nov 2010; revised 18 Jan 2011; accepted 18 Jan 2011; published 28 Jan 2011

substrates and have been so far applied to produce most successful photonic metamaterial designs, like split rings [6,7], nanorod pairs [8], and the fishnet [9]. However top-down methods suffer from fundamental limitation in the achievable spatial resolution and are not amenable to produce metamaterials with complex 3D inclusions as required by the above mentioned applications.

Among several types of chemically synthesized nanostructures, 2D and 3D clusters of self-assembled plasmonic particles are increasingly attracting interest for their use as building blocks for new magnetic and negative index materials (NIMs) at optical frequencies. In fact, in these kind of structures plasmonic particles, that do not directly interact with an incident magnetic field, can be arranged to force the electric field to circulate in the plane orthogonal to the incident magnetic field, inducing an overall magnetic resonance, in accordance with the concept of plasmonic nanorings proposed in [10]. Besides, such a magnetic-based plasmonic resonance coexists with the individual electric resonance supported by each of the nanoparticles composing a cluster.

For example, in [11] it was shown that plasmonic tetrahedral nanoclusters (NCs) support isotropic electric and magnetic resonances in 3D, and that colloidal solutions of gold tetraclusters can in principle have both negative dielectric permittivity and negative magnetic permeability at frequencies between the near-infrared and the optical range. However, the magnetic response was rather weak both because of the impact of gold losses and the relatively low concentration of the suspension.

The use of NCs formed by core-shell nanoparticles attached to silica cores to accomplish an isotropic magnetic response in the visible range has been suggested in [12], where the possibility of realizing an isotropic double-negative medium arranging such NCs in a cubic lattice was also studied. An extension of the planar design [10] to a 3D isotropic magnetic molecule formed by six closely clustered nanoparticles, without the need for a central dielectric core, has also been presented in [13].

The resonant modes of certain planar clusters of self-assembled metal-dielectric spheres have been experimentally investigated in [14] through dark-field spectroscopy measurements, and evidence of electric, magnetic, and Fano-like resonances have been reported, which makes promising the employment of self-assembled NCs as the building blocks for new nanophotonic structures.

In this work we analyze the optical properties of metamaterials formed by close-packed arrangements of plasmonic NCs, which can be easily realized and assembled by current state-of-the-art nanochemistry techniques. Similarly to the structures considered in [12], such NCs are formed by a number of metal nanocolloids enclosed within a thin dielectric shell and attached to a dielectric core of variable size (Fig. 1). An approximate model based on the single dipole approximation (SDA) [15,16] in conjunction with the multipole expansion [17] of the scattered field is used here to evaluate the electric and magnetic polarizabilities of a few sample NCs. Since we aim at obtaining highly isotropic behaviour of the NCs, a most-regular-disposition criterion is applied to locate the particles around the central cores, leading to completely regular or pseudo-regular NCs, depending on the chosen particle number. We consider different NC configurations and we show that the resonances (in particular the electric and magnetic ones) of this kind of structures can be tuned by varying the number of particles, their separation, and the permittivity of the host material. We also show that certain cluster geometries exhibit electric and magnetic resonances in the same frequency range opening the possibility of realizing isotropic NIMs at optical frequencies. Finally, the permittivity and permeability of the composite media formed by a periodical arrangement of NCs are estimated by the Maxwell Garnett homogenization model.

2. Nanocluster modeling

The colloidal silver nanoparticles are evenly distributed around the dielectric core to obtain a compact and regular ensemble. Compactness of NCs is instrumental in minimizing spatial dispersion effects, and therefore particles are closely packed around the central core. As a consequence, the dimension of the silver nanoparticles determines the maximum number of

#137799 - $15.00 USD Received 8 Nov 2010; revised 18 Jan 2011; accepted 18 Jan 2011; published 28 Jan 2011

nanoparticles that are clustered around the core. Three examples of NCs comprising 4, 12 and 48 silver nanoparticles of variable size are illustrated in Fig. 1. For all configurations the overall dimension of the NC is subwavelength and approximately the same (diameter D around 100 nm). Interparticle spacing (d) can be controlled by coating the particles with polymer shells, as shown in Fig. 1(c). This coating can be easily obtained, for example, by using polymers with thiolated linkers to form self-assembled monolayers on the particle surfaces that can be as thin as 2 nm [18], thus providing a very precise control of nanoparticles separations. Charged molecules in solvent or polymers attached to the silver nanospheres can also be used for a few nm separations [19].

NCs can then be built with current nanochemistry technology. Since the particles are dielectric coated, their assembling into clusters around the silica core can be carried out by the same process used in the self-assembly of dielectric-dielectric core-shell clusters [20,21]. Depending on the chosen number of nanoparticles, their positions around the silica core is derived either by an analytical distribution law (regular NCs), assuming that they coincide with the vertices of a Platonic solid (the thetrahedral and icosahedral NCs are shown in Fig. 1 (a) and (b), respectively), or through a numerical procedure (pseudo-regular NCs) maximizing the minimum interparticle distance [22] (Fig. 1(c)). Both approaches used to define particle positions lead to a uniform distribution of the nanoparticles around the central dielectric core, contributing to the desired isotropy of the NC optical response. In particular, maximization of the minimum interparticle distance is equivalent to minimize the total potential energy of repulsion among N unit charges interacting in pairs and constrained to lie on the surface of a sphere [22]. Indeed, for certain number of particles N, the minimum energy configurations correspond to the Platonic solids consisting of equilateral triangles or to some Archimedean semiregular polyhedra or their duals [23]. More generally, most of these configurations have a fairly high order of symmetry [23]. For example, the 48-element arrangement from Fig. 1(c) is highly symmetrical containing two subsets of 24 equivalent points [24].

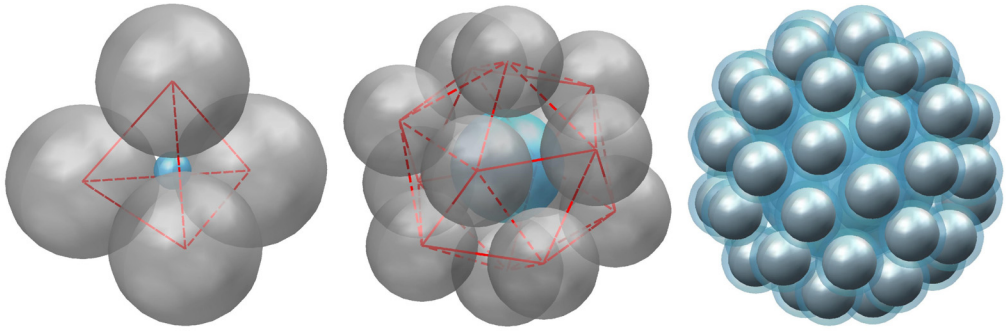

Fig. 1. Examples of NC geometries analyzed in this paper: (a) 4-element tetrahedral and (b) 12-element icosahedral NCs derived by locating nanospheres at the vertices of the respective Platonic solid; (c) 48-element NC with maximized minimum interparticle distance.

There are two main resonant modes of the NCs we are interested in, namely the electric and magnetic dipole resonances [10,12,13]. At the electric resonance, the NC overall induced electric dipole dominates, as a result of the polarization of the silver nanoparticles being mainly parallel to the incident electric field (Fig. 2(a)). At the magnetic resonance, the induced magnetic dipole dominates, and the polarization of the silver nanoparticles wraps around the incident magnetic field. In other words, the applied magnetic field forms, like in [10], effective polarization nanorings around the silica core (Fig. 2(b)). Both electric and magnetic resonances of the NC originate from the combination of plasmonic resonances of the individual nanoparticles.

#137799 - $15.00 USD Received 8 Nov 2010; revised 18 Jan 2011; accepted 18 Jan 2011; published 28 Jan 2011

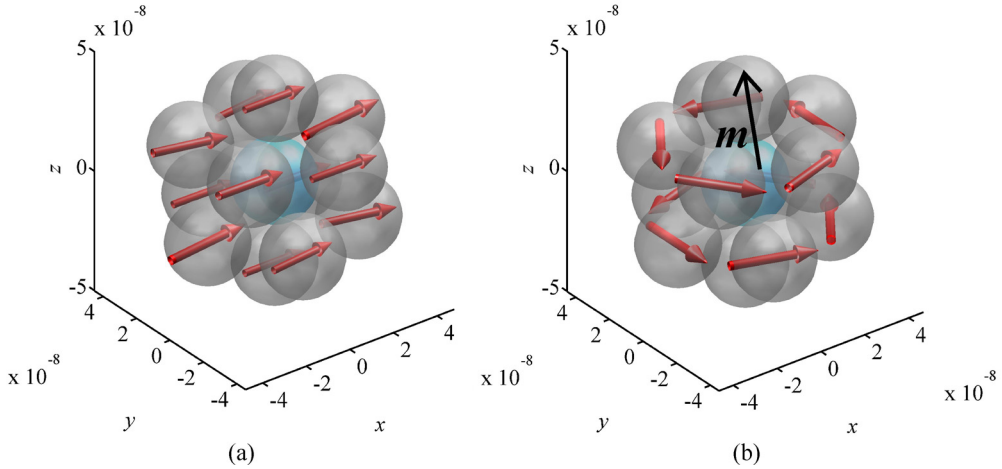

Fig. 2. (a) Electric and (b) magnetic resonant modes for a sample NC.

To characterize the two main resonant modes of a NC, one can use two special configurations of the incident field, so as to isolate either the electric or the magnetic response. Namely, as suggested in [25], one should adopt either an almost uniform electric and vanishing magnetic or an almost vanishing electric and uniform magnetic incident field configurations, respectively. Such configurations can be practically achieved by using a set of plane waves with proper propagation directions and polarizations [25] or through quasistatic electric and magnetic fields [12]. In this paper, we will adopt resonant spherical harmonics to single out the electric and magnetic responses of a NC as in [26]. Indeed, a complete and accurate 3D characterization of the NC optical properties can be achieved by expanding into spherical harmonics the field scattered from a NC illuminated by an arbitrary incident field, and deriving the various equivalent multipoles of the NC. This approach can be applied both when using a full-wave electromagnetic solver and the SDA.

4.1 Spherical wave expansion of the field scattered by the cluster

The spherical wave expansion of the scattered electromagnetic field by a NC outside an enveloping sphere of radius r_0 can be written in the form [17]

$$\begin{aligned}\mathbf{E}(r,\theta,\phi) &= k_h\sqrt{\zeta_h}\sum_{s=1}^{2}\sum_{n=1}^{N}\sum_{m=-n}^{n} Q_{smn}^{(3)}\mathbf{F}_{smn}^{(3)}(r,\theta,\phi),\\ \mathbf{H}(r,\theta,\phi) &= -i\frac{k_h}{\sqrt{\zeta_h}}\sum_{s=1}^{2}\sum_{n=1}^{N}\sum_{m=-n}^{n} Q_{smn}^{(3)}\mathbf{F}_{3-s,m,n}^{(3)}(r,\theta,\phi), \quad r_0 < r < \infty\end{aligned} \tag{1}$$

where the functions $\boldsymbol{F}$ are the spherical harmonics [17], k_h and ζ_h denote the wavenumber and intrinsic impedance of the host medium, respectively, and an $\exp(-i\omega t)$ time harmonic dependence is assumed. The coefficients $Q_{smn}^{(3)}$ of the expansions can be derived by projecting the scattered field onto the spherical harmonics and exploiting the orthogonality properties of the spherical harmonics [17, p. 96]. The truncation limit *N* of the spherical wave expansion, that is the number of terms that must be retained in the expansions for a given accuracy, depends on the size of the NC, and since this is usually small with respect to the wavelength, the number of terms to be considered is limited to a handful.

#137799 - $15.00 USD Received 8 Nov 2010; revised 18 Jan 2011; accepted 18 Jan 2011; published 28 Jan 2011

4.2 SDA and closed-form expression for the spherical coefficients

As customary, in the context of the SDA model [15,16], each metallic nanosphere is simply characterized by its induced electric dipole $\mathbf{p} = \alpha \mathbf{E}_{loc}$, where α is the electric polarizability of the nanosphere and $\mathbf{E}_{loc}$ is the local electric field. For the polarizability of each single nanosphere we use the exact expression obtained from the Mie theory, related to the value of the scattering coefficient of the first spherical mode, that has the following expression [15]

$$\alpha = \frac{6i\pi\varepsilon_0\varepsilon_h}{k^3}\frac{m\psi_1(mka)\psi_1'(ka)-\psi_1(ka)\psi_1'(mka)}{m\psi_1(mka)\xi_1'(ka)-\xi_1(ka)\psi_1'(mka)}, \tag{2}$$

where $\psi_1(\rho) = \rho j_1(\rho) = \sin\rho/\rho - \cos\rho$, $\xi_1(\rho) = \rho h_1^{(1)}(\rho) = (-i/\rho - 1)e^{i\rho}$ denote the Ricatti-Bessel functions, $m = k_m/k = \sqrt{\varepsilon_m/\varepsilon_h}$ is the relative refractive index, $k_m = \omega\sqrt{\varepsilon_m}/c$ is the wavenumber in the metal, a is the radius of the nanosphere, and ε_m and ε_h are the relative permittivity of the metal and of the host medium, respectively. Expressing the local electric field at each nanoparticle as the sum of the incident field and of the contributions of all the other nanoparticles yields an algebraic system of equations, whose solution provides all the nanosphere equivalent dipoles p_q, $q = 1,2,\ldots N_p$ [16,26,27].

The metals are described by a Drude form of the dielectric function, $\varepsilon_m = \varepsilon_\infty - \omega_p^2\left[\omega(\omega + i\gamma)\right]^{-1}$, where ε_∞ is the background permittivity of the metal, ω_p is the plasmon radian frequency and γ is the damping frequency. Silver is simulated using $\varepsilon_\infty = 5$, $\omega_p = 1.37\times10^{16}$ rad/s, and $\gamma = 27.3\times10^{12}\,\mathrm{s}^{-1}$. This parameterization provides a reasonably accurate description of the dielectric properties of silver across the optical range.

For simplifying the analysis, we assume that the host medium and the dielectric core, as well as the possible dielectric coating of nanospheres required to provide interparticle distance, have the same permittivity $\varepsilon_r = 2.2$. Indeed, our model well approximates the case of a glass core, and all clusters immersed in a solvent with such or similar permittivity.

In the context of the SDA we resort to a general representation of the spherical coefficients $Q_{smn}^{(3)}$ expressed in terms of the electric and magnetic currents in the cluster by applying the reciprocity principle [17]

$$Q_{smn}^{(3)} = (-1)^{m+1}\int_V \left(k_h\sqrt{\zeta_h}\,\mathbf{F}_{s,-m,n}^{(1)}\cdot\mathbf{J} + i\frac{k_h}{\sqrt{\zeta_h}}\mathbf{F}_{3-s,-m,n}^{(1)}\cdot\mathbf{M}\right)dV. \tag{3}$$

By using this alternative representation and taking into account that in the SDA the current in the NC coincides with a collection of elementary dipoles

$$\mathbf{J} = -i\omega\sum_{q=1}^{N_p}\mathbf{p}_q(\mathbf{r}_q)\delta(\mathbf{r}-\mathbf{r}_q) \tag{4}$$

we derive the following simple closed-form relation expressing the spherical coefficients relative to the excited NC

$$Q_{smn}^{(3)} = i\omega k_h\sqrt{\zeta_h}(-1)^m\sum_{q=1}^{N_p}\mathbf{F}_{s,-m,n}^{(1)}(\mathbf{r}_q)\cdot\mathbf{p}_q(\mathbf{r}_q). \tag{5}$$

This result makes the combination of the SDA and SWE a very effective tool for the analysis of the optical properties of NCs.

#137799 - $15.00 USD Received 8 Nov 2010; revised 18 Jan 2011; accepted 18 Jan 2011; published 28 Jan 2011

4.3 Extinction and scattering cross sections

To characterize the NC scattering response, it is useful to consider its extinction scattering and absorption cross sections and the corresponding efficiencies, under plane wave illumination. In the context of the SDA the cross section expressions have been summarized in [15,16].

More convenient expressions, that can be used also when the scattered field is computed by full-wave simulations, can be also derived in terms of the spherical coefficients [27]

$$C_{ext} = \frac{\zeta_h}{2|\mathbf{E}_i|^2}\mathrm{Re}\left[\sum_{smn} Q^{(3)}_{smn}\left(Q^{i}_{smn}\right)^*\right], \qquad C_{sca} = \frac{\zeta_h}{2|\mathbf{E}_i|^2}\sum_{smn}\left|Q^{(3)}_{smn}\right|^2, \tag{6}$$

where $|\mathbf{E}_i|$ denotes the electric field strength, and Q^{i}_{smn} the spherical coefficients [17, p. 341] of the incident plane wave. The absorption cross section is obtained as the difference from the extinction and the scattering cross sections

$$C_{abs} = C_{ext} - C_{sca} \tag{7}$$

Extinction, scattering and absorption efficiencies $Q_{ext,sca,abs}$ are evaluated as $Q_{(.)} = C_{(.)}/C_{geom}$ where $C_{geom} = \pi R_e^2$ is the geometrical cross section of the minimal sphere enveloping the cluster ($R_e = a + 2r_p + d$).

4.4 Equivalent dipole and quadruple components of the cluster

Once the scattered field is expanded in spherical harmonics, the various components of the induced electric and magnetic dipole moments excited by an incident electromagnetic field, can be readily calculated in terms of the spherical coefficients through the following relations

$$\begin{aligned} p_e^x &= ic_e\left(Q^{(3)}_{2,1,1} - Q^{(3)}_{2,-1,1}\right), \quad p_e^y = -c_e\left(Q^{(3)}_{2,1,1} + Q^{(3)}_{2,-1,1}\right), \quad p_e^z = -i\sqrt{2}c_e Q^{(3)}_{201}, \\ p_m^x &= c_m\left(Q^{(3)}_{1,1,1} - Q^{(3)}_{1,-1,1}\right), \quad p_m^y = ic_m\left(Q^{(3)}_{1,1,1} + Q^{(3)}_{1,-1,1}\right), \quad p_m^z = -\sqrt{2}c_m Q^{(3)}_{101}, \end{aligned} \tag{8}$$

where $c_e = \sqrt{3\pi}/(\omega k_h\sqrt{\zeta_h})$ and $c_m = \sqrt{3\pi}\sqrt{\zeta_h}/(\omega\mu_0 k_h)$. Expressions (8) can be derived by simply comparing the standard expressions of the electromagnetic field radiated by a short electric or magnetic dipole with the expressions of the spherical wave functions for $n = 1$. Similarly, we can derived the components of the higher order multipole contributions. In particular, taking into account that the field radiated by an electric quadrupole can be represented in terms of solely the $n = 2$ harmonics, the equivalent quadrupole components of the scattered field can be expressed as

$$\begin{aligned} Q_{xx} &= c_q\left[Q^{(3)}_{202} + \sqrt{6}\left(Q^{(3)}_{222} + Q^{(3)}_{2,-2,2}\right)\right], \quad Q_{xy} = -i\sqrt{6}c_q\left(Q^{(3)}_{222} - Q^{(3)}_{2,-2,2}\right), \\ Q_{yy} &= c_q\left[Q^{(3)}_{202} - \sqrt{6}\left(Q^{(3)}_{222} + Q^{(3)}_{2,-2,2}\right)\right], \quad Q_{yz} = \frac{4\sqrt{6}c_q}{14+\sqrt{15}}\left(Q^{(3)}_{212} + Q^{(3)}_{2,-1,2}\right) \\ Q_{zz} &= c_q Q^{(3)}_{202}, \qquad\qquad\qquad\qquad\qquad Q_{xz} = \frac{4\sqrt{6}c_q}{14+\sqrt{15}}\left(Q^{(3)}_{212} - Q^{(3)}_{2,-1,2}\right) \end{aligned} \tag{9}$$

where $c_q = 2\sqrt{30\pi}/\left(i\omega k_h^2\sqrt{\zeta_h}\right)$.

3. Efficiencies and discussion of resonances for a single nanocluster

We now consider three sample NC configurations, with similar overall sizes but differing in metal nanoparticle number and radii, whose optical responses are representative of the broad

#137799 - $15.00 USD Received 8 Nov 2010; revised 18 Jan 2011; accepted 18 Jan 2011; published 28 Jan 2011

class of these structures. In all these configurations, we assume that the metal nanoparticles are coated with 2 nm thick polymer shells to ensure a 4 nm surface-to-surface separation between them, which is large enough to let the dipole-dipole model provide meaningful results and to avoid different scattering mechanisms between particles. Indeed, particle separation does not directly affect SDA results, but for too closely spaced or contacting particles the SDA loses any accuracy [28]. Specifically, the three considered NCs and their geometrical and dimensional characteristics are as follows:

A) Regular tetrahedral NC from Fig. 1(a), formed by 4 solid silver nanospheres of radius a = 22 nm arranged around a central dielectric particle with radius of 5.4 nm, and with overall size of the cluster $D = 2R_e = 106.8$ nm.

B) Icosahedral NC from Fig. 1(b), formed by 12 solid silver nanospheres of radius 16 nm arranged around a central dielectric particle of radius a = 16.2 nm, with overall size of the cluster D = 104.5 nm.

C) Pseudo-regular NC from Fig. 1(c), formed by 48 solid silver particles of radius a = 8 nm attached to a central core of radius 27.7 nm and having an overall size of the cluster D = 95.4 nm.

For all the three NCs, we assume that the central core is made of silica with relative permittivity ε_r = 2.2, and we remind that, similarly to [11], to simplify the calculation we assume that the NCs are immersed in a medium with the same permittivity ε_r = 2.2.

At first, to characterize the frequency position and strength of the NCs resonances, in all the three cases we analyze the extinction, scattering, and absorption efficiencies, when each NC is illuminated by a linearly polarized plane wave. In addition, to identify the nature of the various NC resonances, we decompose the total scattering efficiency into the contributions originated by the induced electric and magnetic dipole moments, $Q_{sca}^{p_e}$ and $Q_{sca}^{p_m}$ respectively, and that associated with all the remaining higher order multipoles Q_{sca}^{mps}, which are plotted separately. The electric and magnetic resonance frequencies correspond to the peaks of $Q_{sca}^{p_e}$ and $Q_{sca}^{p_m}$, respectively. At the same frequencies, the NC absorption also exhibits a maximum as expected at resonance. We recall that the electric resonance has a larger scattering contribution than the magnetic one, since it is associated to a radiating electric dipole, whereas the magnetic resonance radiates as a current loop, which in general exhibit less scattering and higher losses.

Figure 3 shows the extinction, scattering and absorption efficiencies of an isolated tetrahedral NC of type-A. As apparent, the cluster exhibits both an electric and a magnetic resonance that occur at very close frequencies, 594 and 602 THz, respectively. The magnetic resonance frequency is slightly above the electric one, and since the latter is usually stronger and broader than the former, this resonance order opens the possibility to achieve negative permeability at some frequency within the negative permittivity band, and thus a negative index response, provided that the magnetic resonance is strong enough. The scattering efficiency corresponding to the higher order multipoles has a peak at higher frequency.

It is noteworthy that, at the magnetic resonance, coincident with the magnetic dipole efficiency $Q_{sca}^{p_m}$ and that, as expected, the magnetic dipole scattering $Q_{sca}^{p_m}$ is negligible compared to the total scattering efficiency Q_{sca}. Viceversa, at the electric resonance the scattering efficiency Q_{sca} is almost coincident with the electric dipole efficiency $Q_{sca}^{p_e}$, indicating that indeed scattering of the electric resonance is dominant compared to its absorption. In summary, these results clearly show that (i) magnetism is present, and that (ii) absorption at the magnetic and electric frequencies is comparable.

#137799 - $15.00 USD Received 8 Nov 2010; revised 18 Jan 2011; accepted 18 Jan 2011; published 28 Jan 2011

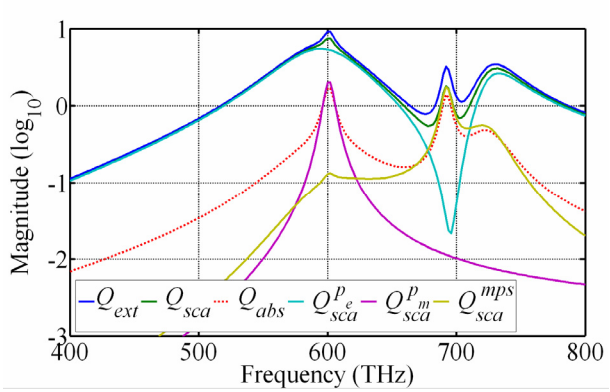

Fig. 3. Extinction, scattering, and absorption efficiencies of the tetrahedral NC type-A.

The plane wave responses of the two other sample NCs type-B and type-C are analyzed in Figs. 4 and 5, respectively. Differently from the case of the tetrahedral NC type-A, the electric and magnetic resonances occur at well separated frequencies for both the icosahedral type-B and the 48-particle type-C NCs, and the frequency of the magnetic resonance is lower than that of the electric resonance. This is seemingly the result of a few concurrent effects. On the one hand, since the magnetic mode is supported by currents circulating around the central dielectric core of the cluster, as schematically shown in Fig. 2, the larger is the size of this current loop (for a fixed gap between contiguous nanospheres), the lower is the magnetic resonant frequency (red shift). Indeed, each of the plasmonic nanorings contributing to the magnetic dipole resembles a split ring with multiple cuts/gaps, and the relevant equivalent total inductance increases for increasing nanoring radii. Moreover, since the sample cluster configurations we are considering (A, B, C) have comparable overall dimensions, the more populated NCs are formed by particles of smaller size, which also contributes to increasing the NC equivalent inductance. On the other hand, the smaller are the nanospheres and the weaker is the capacitive coupling between them, due to the reduced area of facing surfaces. Besides, a larger number of particles, and therefore gaps, in each nanoring corresponds to a larger number of nanocapacitors connected in series, which further decreases the total capacitance of the nanoring (as for split rings with multiple splits [29]); consequently, the magnetic resonance frequency will decrease (blue shift) for increasing particle number and decreasing particle size. While the increment of nanoring inductance is the predominant effect when the size of the dielectric core increases from 5.4 nm, for the tetrahedral NC type-A, to 16.2 nm for the icosahedral NC type-B, the reduction of nanoring capacitance, especially associated with the increment of the number of gaps in the loop, tends to prevail when the number of particles is largely increased. As a result of the balance between these opposite trends the magnetic resonance of the icosahedral cluster occurs at a markedly lower frequency (548 THz) than that of the tetrahedral cluster, whereas the corresponding resonance shift for the 48-particle cluster is limited (590 THz).

#137799 - $15.00 USD Received 8 Nov 2010; revised 18 Jan 2011; accepted 18 Jan 2011; published 28 Jan 2011

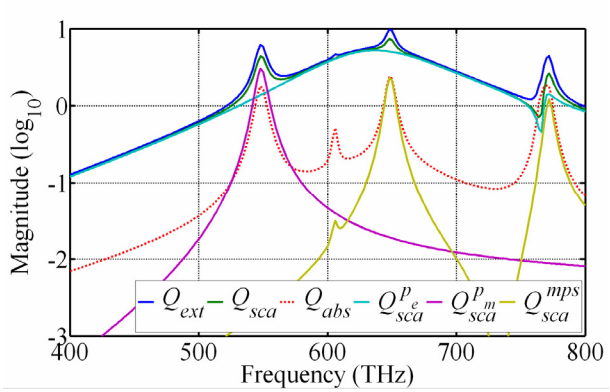

Fig. 4. Extinction, scattering, and absorption efficiencies of the icosahedral NC type-B.

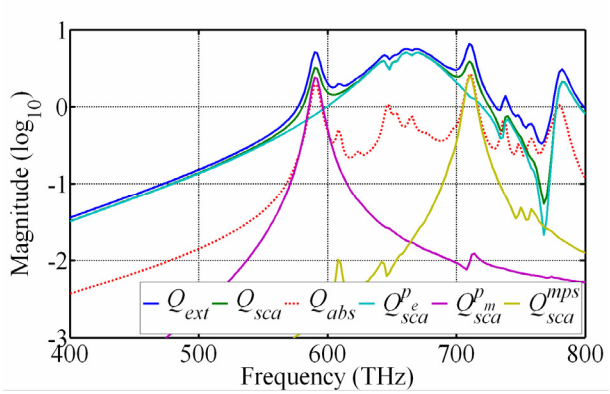

Fig. 5. Extinction, scattering, and absorption efficiencies of the pseudo-regular NC type-C.

Concerning the electric resonance, for a given separation between the particles, this is essentially related to the size of a single particle and increasingly blue-shifts for decreasing particle radii, as apparent from Figs. 4 and 5. Accordingly, the electric resonance frequency of the NC type-C is larger than that of the NC type-B.

Based on the previous observation about the strength and width of electric and magnetic resonances, to engineer a NIM the positions of resonances in those clusters formed by a larger number of particles should be possibly reordered. Tuning of resonances can be achieved by changing the separation between the particles and the dielectric environment of the cluster, and using more complex individual particle and cluster geometries [11,12,14].

These numerical examples also show that the scattering from higher order multipole moments induced by a plane wave usually becomes appreciable at frequencies higher than that of the magnetic resonance. Indeed, Q_{sca}^{mps} practically coincides with the scattering of the effective electric quadrupole moment, because the contribution from multipoles of order higher than the quadrupole is completely negligible in the considered frequency range. At any rate, at low frequencies even the quadrupole moment contribution is considerably smaller than those of the effective electric and magnetic dipoles, as expected from the subwavelength size of the NCs. This ensures a weak spatial dispersion for the NCs, and in turn for the artificial materials obtained by their collection, at electric and magnetic resonances. In this connection, it is noteworthy that, in principle, to further reduce the quadrupole moment in the range of the electric and magnetic dipole resonances, and thus spatial dispersion effects, one could consider to decrease the size of the NCs by employing smaller constituent nanoparticles. However, besides shifting both the electric and magnetic dipolar resonances to higher frequencies, this would inevitably reduce their strength. In particular, the frequency

#137799 - $15.00 USD Received 8 Nov 2010; revised 18 Jan 2011; accepted 18 Jan 2011; published 28 Jan 2011

and strength of the magnetic resonance are closely related to the size of the plasmonic nanorings contributing to the equivalent magnetic dipole of the NCs, as previously pointed out, and artificial magnetism will tail off for increasingly smaller electrical sizes of the NCs.

A further disadvantage related to the use of very small nanoparticles is the increase of losses occurring when the particle size becomes comparable to the electron mean free path. To sum up, the range of particle sizes considered here represents a kind of compromise between the need to obtain significant electric and magnetic responses while limiting spatial dispersion effects. To reduce the overall size of the NCs without compromising their magnetic and electric responses, individual particles with different shapes might possibly be used, but such an investigation is beyond the scope of this work.

4. Polarizability and isotropy properties of a single nanocluster

Based on the analysis detailed above and the observation that in the NCs examined here the electric quadrupole moment does not play a major role, the electric and magnetic dipoles induced in each NC can be generally expressed in terms of the local electric and magnetic fields as

$$\begin{bmatrix} \mathbf{p}_e \\ \mathbf{p}_h \end{bmatrix} = \bar{\mathbf{a}} \begin{bmatrix} \mathbf{E}_{loc} \\ \mathbf{H}_{loc} \end{bmatrix} = \begin{bmatrix} \bar{\mathbf{a}}_{ee} & \bar{\mathbf{a}}_{em} \\ \bar{\mathbf{a}}_{me} & \bar{\mathbf{a}}_{mm} \end{bmatrix} \begin{bmatrix} \mathbf{E}_{loc} \\ \mathbf{H}_{loc} \end{bmatrix}, \tag{10}$$

where the generalized polarizability tensor $\bar{\mathbf{a}}$ is a 6x6 matrix taking into account also possible magneto-electric coupling effects in accordance with the bianisotropic formalism [30]. However, anticipating what shown next, magneto-electric effects $\bar{\mathbf{a}}_{em}, \bar{\mathbf{a}}_{mm}$ are negligible in (11) because of substantial symmetry and subwavelength dimension of the NC.

To single out the various components of the polarizability tensor, we illuminate an isolated cluster with an appropriate superposition of spherical harmonics for $n = 1$, so as to form either an electric or magnetic excitation polarized along three orthogonal directions. Accordingly, six incident waves are used to evaluate the polarizability tensors $\bar{\mathbf{a}}_{ee}, \bar{\mathbf{a}}_{me}$ and $\bar{\mathbf{a}}_{em}, \bar{\mathbf{a}}_{mm}$. For each illuminating wave, by analyzing the NC scattered field, we can evaluate six elements (column) of the polarizability tensor $\bar{\mathbf{a}}$, i.e. three elements (a column) of the electric or magnetic polarizabilities and three elements (a column) of the magneto-electric polarizabilities, that will be simply given by the expressions (8) and (9) of the induced dipoles divided by the field amplitude at the cluster center. In particular, by exciting a NC with the "electric-type" spherical field $\mathbf{E} = k_h\sqrt{\zeta_h}\left[\mathbf{F}^{(1)}_{2,-1,1}(\mathbf{r}) - \mathbf{F}^{(1)}_{2,1,1}(\mathbf{r})\right], \mathbf{H} = k_h\left(i\sqrt{\zeta_h}\right)^{-1}\left[\mathbf{F}^{(1)}_{1,-1,1}(\mathbf{r}) - \mathbf{F}^{(1)}_{1,1,1}(\mathbf{r})\right]$, we provide a practically uniform illumination of a NC with an electric field $\mathbf{E}$ mainly along x, and a magnetic field $\mathbf{H}$ vanishing at the origin $\mathbf{r} \equiv \mathbf{0}$ and remaining negligible in the whole NC volume. With this excitation we determine the polarizability column elements $a^{xx}_{ee}, a^{yx}_{ee}, a^{zx}_{ee}$, and $a^{xx}_{me}, a^{yx}_{me}, a^{zx}_{me}$ by looking at the electric and magnetic dipolar scattered fields terms that lead to (8) and (9). Viceversa, by exciting a NC with the "magnetic-type" spherical field $\mathbf{E} = k_h\sqrt{\zeta_h}\left[\mathbf{F}^{(1)}_{1,-1,1}(\mathbf{r}) - \mathbf{F}^{(1)}_{1,1,1}(\mathbf{r})\right]$, $\mathbf{H} = k_h\left(i\sqrt{\zeta_h}\right)^{-1}\left[\mathbf{F}^{(1)}_{2,-1,1}(\mathbf{r}) - \mathbf{F}^{(1)}_{2,1,1}(\mathbf{r})\right]$ we provide a practically uniform illumination of a NC with a magnetic field $\mathbf{H}$ mainly along x, and an electric field $\mathbf{E}$ vanishing at the origin $\mathbf{r} \equiv \mathbf{0}$ and remaining negligible in the whole NC volume. With this excitation we determine the column polarizability elements $a^{xx}_{mm}, a^{yx}_{mm}, a^{zx}_{mm}$, and $a^{xx}_{em}, a^{yx}_{em}, a^{zx}_{em}$ by looking again at the electric and magnetic dipolar scattered fields terms. Analogously, the excitations consisting of $\mathbf{E} = k_h\sqrt{\zeta_h}\left[\mathbf{F}^{(1)}_{2,-1,1}(\mathbf{r}) + \mathbf{F}^{(1)}_{2,1,1}(\mathbf{r})\right]$, $\mathbf{H} = k_h\left(i\sqrt{\zeta_h}\right)^{-1}\left[\mathbf{F}^{(1)}_{1,-1,1}(\mathbf{r}) + \mathbf{F}^{(1)}_{1,1,1}(\mathbf{r})\right]$, and $\mathbf{E} = k_h\sqrt{\zeta_h}\mathbf{F}^{(1)}_{2,0,1}(\mathbf{r})$, $\mathbf{H} = k_h\left(i\sqrt{\zeta_h}\right)^{-1}\mathbf{F}^{(1)}_{1,0,1}(\mathbf{r})$, produce practically uniform electric fields mainly along y and z, respectively, with associated vanishing magnetic fields, and allows the calculation of the second and third columns of

#137799 - $15.00 USD Received 8 Nov 2010; revised 18 Jan 2011; accepted 18 Jan 2011; published 28 Jan 2011

polarizability tensors $\bar{\mathbf{a}}_{ee}, \bar{\mathbf{a}}_{me}$. Finally, the excitations $\mathbf{E} = k_h \left(\sqrt{\zeta_h}\right)^{-1} \left[\mathbf{F}^{(1)}_{1,-1,1}(\mathbf{r}) + \mathbf{F}^{(1)}_{1,1,1}(\mathbf{r})\right]$, $\mathbf{H} = k_h \left(i\sqrt{\zeta_h}\right)^{-1} \left[\mathbf{F}^{(1)}_{2,-1,1}(\mathbf{r}) + \mathbf{F}^{(1)}_{2,1,1}(\mathbf{r})\right]$, and $\mathbf{E} = k_h \sqrt{\zeta_h} \mathbf{F}^{(1)}_{1,0,1}(\mathbf{r})$, $\mathbf{H} = k_h \left(i\sqrt{\zeta_h}\right)^{-1} \mathbf{F}^{(1)}_{2,0,1}(\mathbf{r})$, produce practically uniform magnetic fields mainly along y and z, respectively, with associated vanishing electric fields, and allows the calculation of the second and third columns of polarizability tensors $\bar{\mathbf{a}}_{em}, \bar{\mathbf{a}}_{mm}$.

Figure 6 shows the polarizabilities calculated for the NC type-A. To make easier the comparison among various contributions, the plots are normalized to have all the same physical dimension (m^3). Namely, $\bar{\mathbf{a}}_{ee}$, $\bar{\mathbf{a}}_{em}$, and $\bar{\mathbf{a}}_{me}$ are normalized by $\varepsilon_0 \varepsilon_h$, v_h^{-1}, and ζ_h^{-1}, respectively, where v_h denotes the light velocity in the host medium. From Fig. 6 it can be observed that the tetrahedral NC type-A exhibits both electric and magnetic responses and the positions of the resonances are consistent with the plot of the scattering efficiencies in Fig. 4. As a consequence of the cluster spherical symmetry, the off-diagonal terms of the electric and magnetic polarizability tensors vanish, while the diagonal ones are practically identical. Moreover, the magneto-electric terms appear to be several orders of magnitude smaller than the non-vanishing (diagonal) terms of the electric and magnetic polarizabilities. Indeed, as pointed out in [11], a tetrahedral cluster is the minimal non-bianisotropic, fully isotropic metamaterial inclusion.

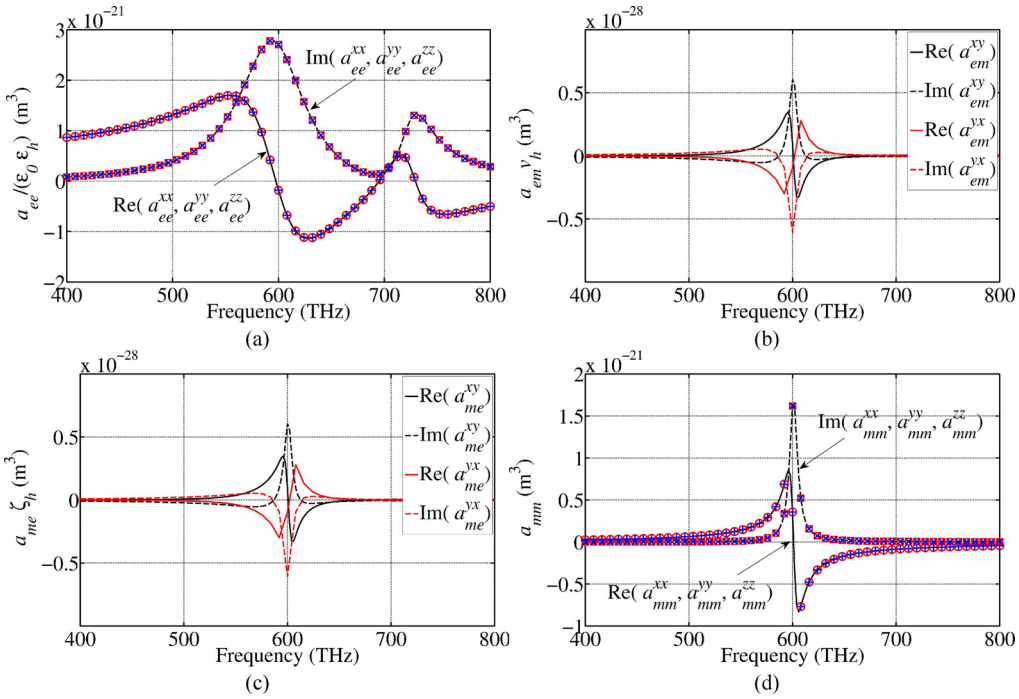

Fig. 6. Polarizabilities of the tetrahedral NC type-A. (a) Electric, (b)-(c) magneto-electric, and (d) magnetic polarizabilities.

The polarizabilities of the NCs type-B and type-C are shown in Figs. 7 and 8, respectively. The optical responses of these clusters display certain common features with that of the NC type-A. Indeed, also these configurations present an isotropic polarizability. Magneto-electric polarizbilities for the NC type-B are even smaller than in the NC type-A, because of the higher degree of symmetry of this configuration. Conversely, in NC type-C the non-perfectly regular particle disposition results in a less effective cancellation of magneto-electric coupling. At any rate, even for the pseudo-regular NC type-C, that can be

#137799 - $15.00 USD Received 8 Nov 2010; revised 18 Jan 2011; accepted 18 Jan 2011; published 28 Jan 2011

representative of structures realizable in practice, magneto-electric polarizabilities are about two orders of magnitude below the diagonal terms of the polarizability tensor.

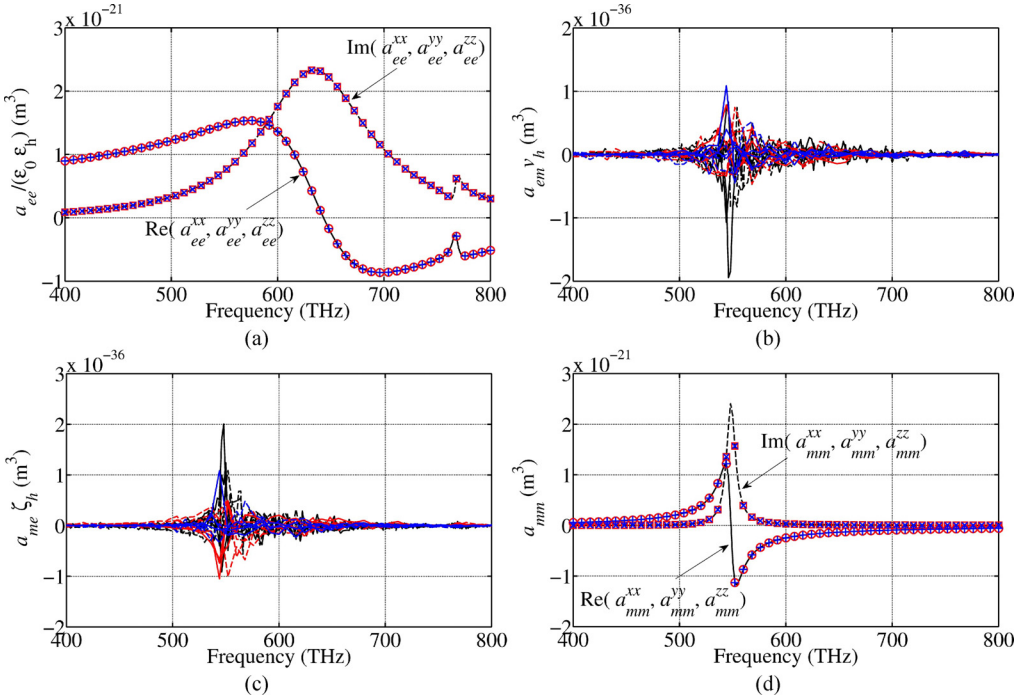

Fig. 7. Polarizabilities of the icosahedral NC type-B. (a) Electric, (b)-(c) magneto-electric, and (d) magnetic polarizabilities.

Indeed, a comprehensive description of the scattering properties of the considered NCs and, in particular, a measure of their optically isotropy can be deduced by examining the NC scattering matrices. It is well-known that the scattering by an isotropic sphere does not mix electric and magnetic degrees of freedom, i.e., there is no coupling between the two fundamental polarizations, nor does it mix multipole orders. As a result, the scattering matrix for an isotropic sphere takes a diagonal form with elements generally referred to as Mie coefficients [15]. On the other hand, anisotropy or arbitrary shape of the scatterer can mix multipole orders as well as electric and magnetic degrees of freedom, and the scattering matrix is generally full. However, the proposed spherical NCs have sufficient symmetry to considerably reduce the number of independent, nonzero scattering matrix elements. Symmetry along with the subwavelength size of NCs contribute to the diagonality of the block of scattering coefficients corresponding to the lowest degree $n=1$ wave functions and to the negligibility of higher order multipoles, such that NCs scattering is analogous to the scattering from a small isotropic sphere. This holds true for both the completely regular NCs based on Platonic solids, as well as the pseudo-regular minimum energy NCs, which possess specific symmetry properties depending on the number of constituent particles [23].

The higher is the symmetry degree of a NC, and more closely its scattering behaviour resembles that of an isotropic sphere. This is clearly illustrated in Fig. 9 showing the spherical wave spectral footprint (i.e. the amplitude of the scattering coefficients) calculated at a sample frequency of 600 THz. Spherical coefficients are indexed by using the convention used in [17] to convert the index triplet (s,m,n) to the single index $j=2\left[n(n+1)+m-1\right]+s$, and responses to wave functions with degree up to $N=5$ are considered.

#137799 - $15.00 USD Received 8 Nov 2010; revised 18 Jan 2011; accepted 18 Jan 2011; published 28 Jan 2011

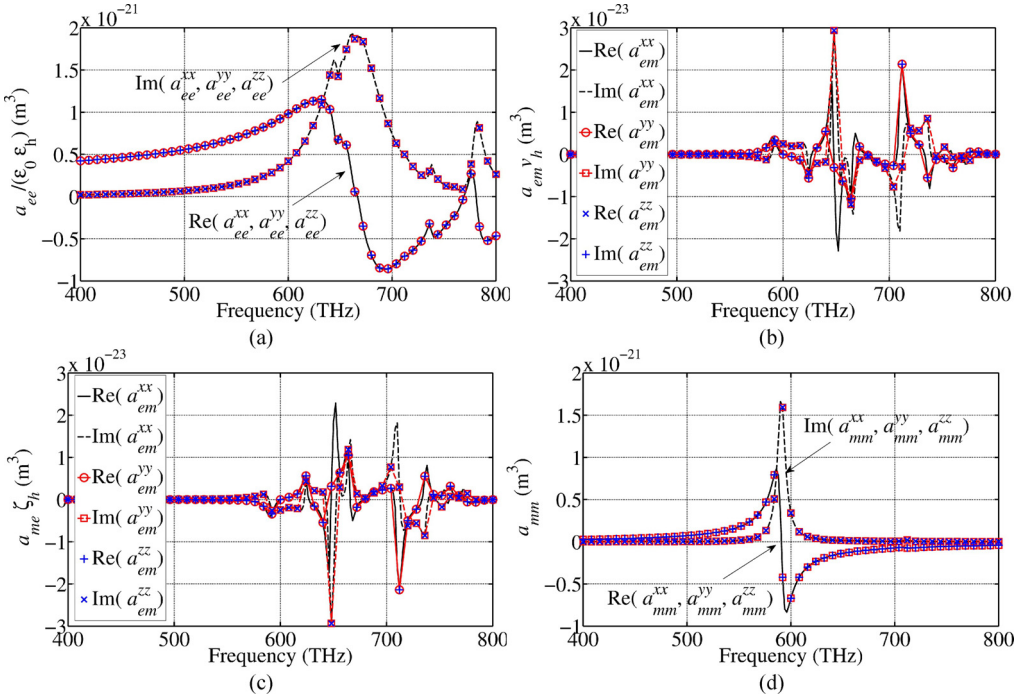

Fig. 8. Polarizabilities of the pseudo-regular NCtype-C. (a) Electric, (b)-(c) magneto-electric, and (d) magnetic polarizabilities.

It can be observed that for the tetrahedral and icosahedral NCs type-A and type-B all of the 30 off-diagonal elements of the first 6×6 minor of the scattering matrix (i.e., entries $n = n' = 1$ corresponding to the electric and magnetic dipole scattering coefficients) are practically zero (<–100 dB), whereas for the NC type-C there are few nonzero off-diagonal coefficients, close to the main diagonal, but their amplitudes are about 50 dB smaller than those of the diagonal elements. It is also evident that very few off-diagonal scattering coefficients corresponding to wave functions with larger degree ($n \geq 2$) are nonzero. In particular, for the icosahedral NC type-B the scattering matrix is perfectly diagonal up to wave functions with degree $n = 3$, while the few off-diagonal coefficients of larger degrees have negligible amplitudes (< –60 dB).

A rigorous demonstration of the relation between geometrical symmetries of the NCs and symmetry properties of the scattering matrix and identification of its non-vanishing elements can be derived in the framework of point group theory, by enforcing the invariance of the scattering matrix under the symmetry operations of the point group the various NCs belong. The derivation is straightforward but tedious and is not reported herein, since the plots in Fig. 9 contain all the relevant information we need for the subsequent developments.

#137799 - $15.00 USD Received 8 Nov 2010; revised 18 Jan 2011; accepted 18 Jan 2011; published 28 Jan 2011

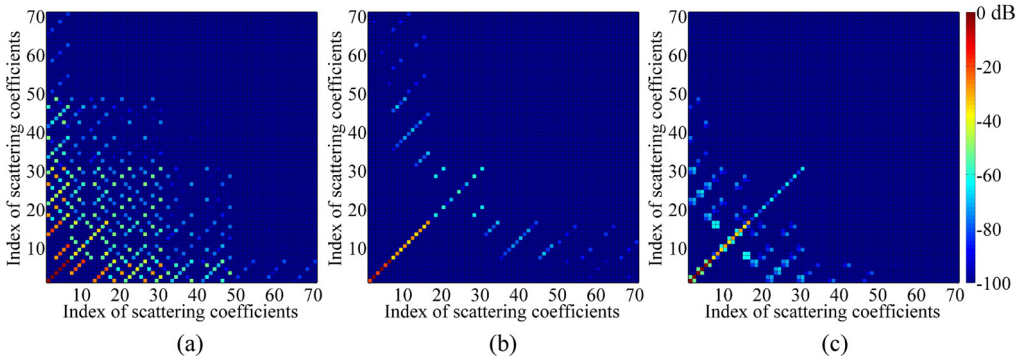

Fig. 9. Spherical wave spectral footprint ($N = 5$) calculated at 600 THz for NCs (a) type-A, (b) type-B, and (c) type-C. Colorbar unit is dB.

We can finally conclude this section recognizing that single NC polarizabilities are orientation independent and mainly non-bianisotropic and, as such, the more general relation (10) can be simplified to the form $\mathbf{p}_e = a_{ee}\mathbf{E}_{loc}$ and $\mathbf{p}_m = a_{mm}\mathbf{H}_{loc}$. In this respect, it must be noted that strictly speaking, the isotropy and non-bianisotropy properties of the NCs would not be sufficient conditions for a homogeneous description in terms of permittivity and permeability of a composite NC aggregates medium. However, provided the lattice has enough symmetries, the size of NCs is truly subwavelength (to avoid spatial dispersion), and magneto-electric coupling among different NCs are negligible, we can assume that periodically arranged cluster composites can be described by scalar effective permittivity (ε_r^{eff}) and permeability (μ_r^{eff}) only. Estimations of such scalar quantities will be presented in the next section comparing the results obtained from the standard Maxwell Garnett homogenization formulas and the expressions developed in [31] for the effective parameters of large filling fraction arrays.

5. Homogenization of collections of nanoclusters: permittivity and permeability

To estimate the effective permittivity and permeability of artificial composite media the extended Maxwell Garnett theory is commonly used [10,12]. In fact, the extended Maxwell Garnett theory incorporates characteristics of Mie scattering in the formulas of the effective permittivity and permeability, expanding their range of validity to arbitrary wavelengths and skin depths within the particles from the original static limit for the ordinary Maxwell Garnett formulas. In particular, it was shown in [31] that the extended Maxwell Garnett effective dielectric permittivity and magnetic permeability correspond to the leading order in the expansion of the exact effective permittivity of a composite of spherical particles in the powers of the filling fraction f, accounting for lattice interactions in the dipole approximation, that is neglecting the effect of higher order multipoles [31].

The usual assumptions for the validity of the Maxwell Garnett type of composite geometry, besides the sizes of the inclusions and distances between them being much smaller than the optical wavelength, and the spherical or ellipsoidal shape of inclusions, require that the distance between the inclusions is much larger than their characteristic size.

In order to obtain a strong magnetic response and negative permeability, the collection of NCs should be rather dense. In the following, we consider 3D periodic arrays arranged in closed-packed face centered cubic (fcc) lattices providing the largest filling fraction value $f = f_{fcc} \sim 0.74$, whereas for simple cubic and body centered cubic (bcc) lattices the maximum filling fraction is $f_{\max} \sim 0.52$ and $f_{\max} \sim 0.68$, respectively.

In principle the Maxwell Garnett model would not be applicable to arrays with such large filling fractions, when the distance between the inclusions is comparable with their characteristic size. Therefore, to estimate the effective medium parameters, we use the

#137799 - $15.00 USD Received 8 Nov 2010; revised 18 Jan 2011; accepted 18 Jan 2011; published 28 Jan 2011

expressions derived from Waterman and Pedersen [31] in the form of expansions of the exact effective permittivity and permeability of a cubic lattice of particles in the powers of the filling fraction *f*. These formulas are valid for any type of cubic lattices (simple cubic, body centered cubic, and face centered cubic) and are correct to terms of order f^6, taking into account higher order multipole effects (lattice interactions), and therefore can provide a more accurate estimation of the effective parameters of close-packed arrays. The effective permittivity and permeability from [31] read as

$$\varepsilon_r^{eff} = \varepsilon_h \left(1 - \frac{3}{2} \frac{t_1^e f}{G^e} \right), \quad \mu_r^{eff} = \left(1 - \frac{3}{2} \frac{t_1^h f}{G^h} \right) \tag{11}$$

with

$$G^v = 1 + \frac{t_1^v f}{2} - t_1^v f \left[\frac{6 t_3^v \sigma_{04}^2 \left(\frac{3f}{4\pi\alpha} \right)^{\frac{10}{3}}}{1 + 15 t_3^v \sigma_{06} \left(\frac{3f}{4\pi\alpha} \right)^{\frac{7}{8}}} + \frac{220}{3} t_5^v \sigma_{06}^2 \left(\frac{3f}{4\pi\alpha} \right)^{\frac{14}{3}} + \frac{1120}{33} t_7^v \sigma_{08}^2 \left(\frac{3f}{4\pi\alpha} \right)^6 \right] \tag{12}$$

for $v = e, h$. In (11) and (12) the coefficients t_n^v are related to the diagonal elements of the scattering matrix by

$$t_1^v = \frac{3i}{(k_h R_e)^3} \frac{S_{s11;s11}}{1 + S_{s11;s11}}, \quad t_n^v = \frac{2i(2n)!(2n+1)!}{(n!)^2 (2k_h R_e)^{2n+1}} S_{s1n;s1n}, \quad n = 3, 5, 7 \tag{13}$$

where $s = 2, 1$ for $v = e, h$, respectively, α is the number of particles per unit cell, and σ_{mn} denote the normalized lattice sums, whose values for the various type of cubic lattices (sc, bcc, and fcc) can be found in [31].

Expressions (11) were originally developed for composite of spheres, but their application can be extended to arrays of spherical NCs once we have recognized that their scattering behavior in the frequency range of interest is very analogous to that of a sphere, as shown in Fig. 9. Moreover, in (13) we have referred to the scattering coefficients corresponding to field polarization along the x- or y-axis (m = 1), but due to the substantial isotropy of the considered NCs, the coefficients with m = 0 could be equivalently used.

It is noted that upon neglecting the higher order multipole coefficients, namely by assuming $G^v = 1 + t_1^v f/2$, (11) exactly reduce to the Maxwell Garnett formulas. Therefore, it is expected that if higher order multipoles are weakly excited, the correction provided by (11) to Maxwell Garnett model estimations would be very limited. As a check, in the following examples along with the results calculated by (11), which will be denoted in the graphs as "WP", we report also those obtained from Maxwell Garnett formulas (denoted by "MG"). It will be shown that Maxwell Garnett formulas hold reasonably well even for close packing of the constituent particles, in accordance with the comparisons performed in [32–34] against direct calculations for periodic and random arrangements of dielectric and metallic spheres. Note that in (13) the definitions of t_1^e and t_1^h take into account the subtraction of the dipolar radiative loss term $-ik_h^3/(6\pi)$ in accordance with the cancellation of scattering losses in a periodic metamaterial [35], whereas our procedure leading to the scattering coefficients includes all radiation losses.

In Fig. 10 we show the effective permittivity and permeability of a composite formed by a periodical arrangement of the tetrahedral NC type-A. We assume the filling fraction to be *f* = 0.74, corresponding to close-packed fcc lattice. First it is noted that results from expansions (11), plotted in red, are exactly superimposed with those obtained from Maxwell Garnett

#137799 - $15.00 USD Received 8 Nov 2010; revised 18 Jan 2011; accepted 18 Jan 2011; published 28 Jan 2011

(MG) model, plotted as black lines. Consistently with the preceding analysis of the extinction and scattering efficiencies, the magnetic permeability exhibits a resonance at a frequency slightly above the resonance of the effective permittivity. As apparent, the strong electric resonance provides very large positive and negative values of the permittvity also for the lattice with lower cluster concentration (simple cubic lattice). Though absorption losses are significant at the electric resonance, as the large imaginary part of the effective permittivity reveals, slightly away from the resonance there are broad frequency ranges where extreme values of the permittivity can be exploited with negligible losses. The magnetic resonance is weaker than the electric one, but strong enough to make the permeability reach negative values. It is also noted that the magnetic resonance falls within the negative region of the effective permittivity, so that a negative index behaviour can be achieved.

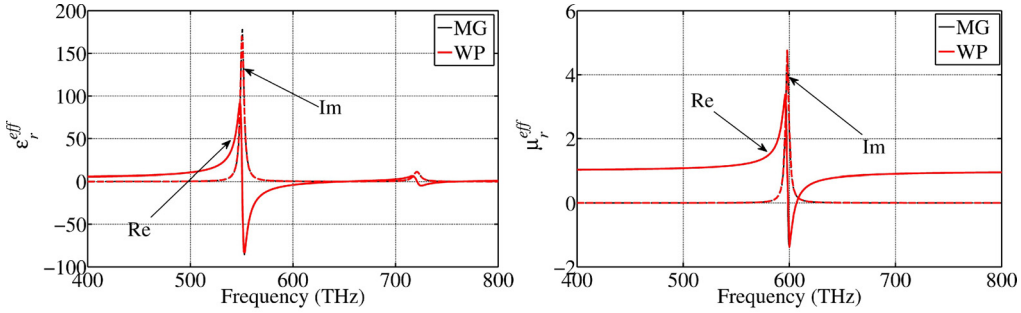

Fig. 10. (a) Permittivity and (b) permeability of a close-packed 3D periodic fcc array of tetrahedral NCs type-A calculated by MG (black lines) and WP (red lines) formulas. Real and imaginary parts of the parameters are shown in solid and dashed lines, respectively.

Next, we examine the effective parameters of a periodic arrangement of the icosahedral NCs type-B that are plotted in Fig. 11. Results from expansions (11) are very close to those obtained from Maxwell Garnett model. As in the previous composite, we observe resonant responses of both the permittivity and permeability, that soon after the resonance reach large negative values. Indeed, the magnetic resonance is even stronger than in the tetrahedral NC medium. However, the positions of the electric and magnetic resonances is exchanged and more spaced apart with respect to the previous case, as we have also observed in Fig. 4. Therefore the resonance bands are not sufficiently overlapped to simultaneously have $\mathrm{Re}(\varepsilon_r^{eff}) < 0$ and $\mathrm{Re}(\mu_r^{eff}) < 0$. As aforementioned, reordering of resonances could possibly be accomplished by increasing the particle separation, since interaction of particles more strongly affects the magnetic resonance, or substituting the central dielectric core with a core-shell particle [12].

In Fig. 12 are shown the effective parameters of a composite made by a periodical arrangement of NCs type-C. Also in this case the results from Maxwell Garnett model are in almost perfect agreement with those from Waterman and Pedersen expansions. The electric and magnetic resonances, previously identified from the analysis of the extinction and scattering efficiencies, lead to resonant behaviors of both the effective permittivity and permeability. The order of the resonances is the same as in the composite of NCs type-B, though both shifted at higher frequencies.

In Fig. 13 we report the effective material parameters of a 3D collection of tetrahedral NCs made of particles with a radius smaller than in the initial NC type-A (11 nm instead 22 nm), such that the overll size of the NCs is now $D = 57.8$ nm. Effectve permittivity and permeability are calculated by the Waterman and Pedersen expressions. The lattice is of the fcc type, as in the previous examples. As expected, both the electric and magnetic resonances are shifted to higher frequencies. Moreover, the strength of the resonances is decreased. This reduction is more significant for the magnetic resonance, and as a consequence the permeability no longer assumes negative values in any frequency range. As mentioned above,

#137799 - $15.00 USD Received 8 Nov 2010; revised 18 Jan 2011; accepted 18 Jan 2011; published 28 Jan 2011

the magnetic activity is produced by the plasmonic nanorings forming the NCs, and the scattered magnetic field is proportional to the area of the current loops they support. Therefore, reducing the NC size determine a corresponding geometrical reduction of the intensity of the magnetic response, which precludes the possibility of achieving negative permeability in collections of too small NCs.

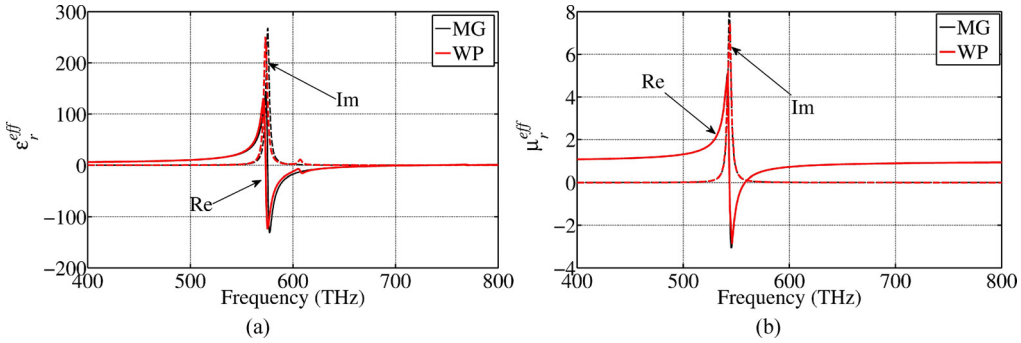

Fig. 11. As in Fig. 9, but for a close-packed 3D periodic fcc array of icosahedral NCs, type-B.

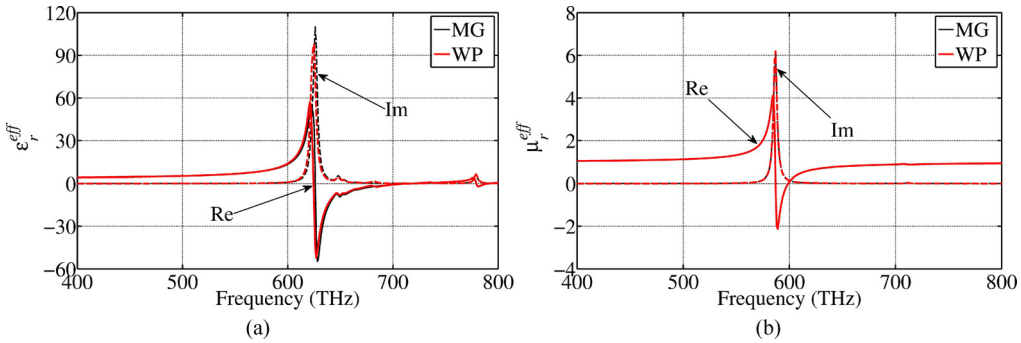

Fig. 12. As in Fig. 9 or 10, but for close-packed 3D periodic arrays of pseudo-regular NCs type-C.

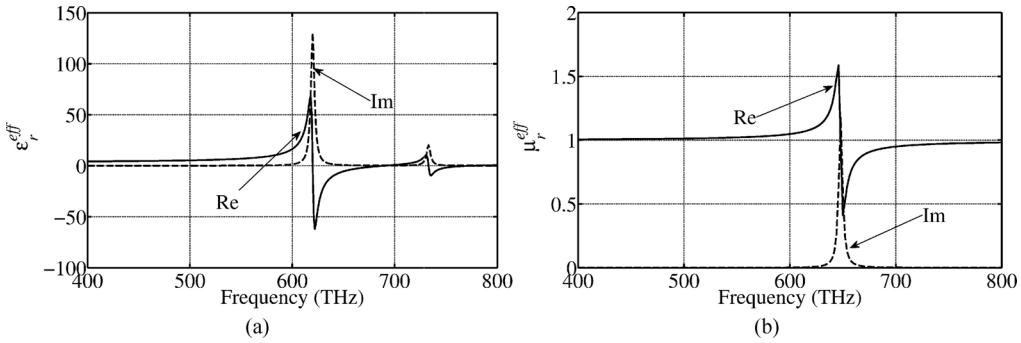

Fig. 13. As in Fig. 9, but here the radius of silver nanospheres is 11 nm and the overall dimension of an individual tetrahedral cluster is $D = 57.8$ nm.

6. Conclusion

We have examined the optical properties of 3D metamaterials formed by close-packed arrangements of plasmonic NCs formed by a number of core-shell metal-dielectric nanocolloids attached to a central dielectric core, that can be easily realized and assembled by current state-of-the-art nanochemistry techniques. A most-regular-disposition criterion is applied to locate the particles around the central cores in order to obtain highly isotropic

#137799 - $15.00 USD Received 8 Nov 2010; revised 18 Jan 2011; accepted 18 Jan 2011; published 28 Jan 2011

behavior of the NCs. By combining a SDA with the SWE of the scattered field we have shown that 3D nanoclusters are useful for creating isotropic electric and magnetic activity which can be tuned and even superimposed by proper design of the NC. Such electric and magnetic activities are inherited by the composite material created by packing NCs. The material properties of the periodic arrays of NCs have been estimated by both the widely used Maxwell Garnett model and the more accurate Waterman-Pedersen model, for a better description of particle interactions for dense arrangements. However, results from the two models were found in very good agreement. Finally, it must be pointed out that the results obtained for the material parameters of nanocluster arrays are based on the approximate Drude model for the dielectric constant of silver, and on the use of approximate homogenization techniques; therefore these values, though rather promising, will need further validation by more extended and accurate simulations and experimental check.

Acknowledgment

The authors acknowledge partial support from the European Commission 7th Framework Program FP7/2008, "Nanosciences, Nanotechnologies, Materials and New Production Technologies (NMP)" theme, research area "NMP-2008-2.2-2 Nanostructured meta-materials", grant agreement number n° 228762.

#137799 - $15.00 USD Received 8 Nov 2010; revised 18 Jan 2011; accepted 18 Jan 2011; published 28 Jan 2011